Effect of Cholesterol on the Biophysical and Physiological Properties of a Clinical Pulmonary Surfactant

Eleonora Keating,* Luna Rahman,* James Francis,† Anne Petersen,† Fred Possmayer,§ Ruud Veldhuizen,‡ and Nils O. Petersen*¶

*Department of Chemistry; †Surface Science Western, Western Science Centre; ‡Departments of Physiology and Pharmacology and Medicine, Lawson Health Research Institute, and §Department of Obstetrics and Gynecology, London Health Sciences Centre, University of Western Ontario, London, Canada; and ¶National Institute for Nanotechnology, National Research Council Canada, Edmonton, Canada

ABSTRACT Pulmonary surfactant is a complex mixture of lipids and proteins that forms a surface-active film at the air-water interface of alveoli capable of reducing surface tension to near 0 mN/m. The role of cholesterol, the major neutral lipid component of pulmonary surfactant, remains uncertain. We studied the physiological effect of cholesterol by monitoring blood oxygenation levels of surfactant-deficient rats treated or not treated with bovine lipid extract surfactant (BLES) containing zero or physiological amounts of cholesterol. Our results indicate no significant difference between BLES and BLES containing cholesterol immediately after treatment; however, during ventilation, BLES-treated animals maintained higher PaO_2 values compared to BLES + cholesterol-treated animals. We used a captive bubble tensiometer to show that physiological amounts of cholesterol do not have a detrimental effect on the surface activity of BLES at 37°C. The effect of cholesterol on topography and lateral organization of BLES Langmuir-Blodgett films was also investigated using atomic force microscopy. Our data indicate that cholesterol induces the formation of domains within liquid-ordered domains (L_o). We used time-of-flight-secondary ion mass spectrometry and principal component analysis to show that cholesterol is concentrated in the L_o phase, where it induces structural changes.

INTRODUCTION

Pulmonary surfactant is a complex mixture of lipids and proteins that is secreted by alveolar type II epithelial cells and adsorbs to the lung air-water interface, where it forms a surface-active film. The film reduces the work of breathing by lowering the surface tension during inspiration. This film can also attain surface tension of near 0 mN/m during expiration and in doing so prevent alveolar collapse at low lung volumes.

Surfactant is essential for normal lung function. Premature babies who do not have sufficient amounts of surfactant can develop respiratory distress syndrome (RDS), a leading cause of neonatal mortality. Exogenous surfactant is administered to treat this condition. As well, surfactant treatment has been investigated with patients with acute lung disease and acute RDS (1–3).

The chemical composition of pulmonary surfactant is highly conserved among different animal species. It consists of 80–90% phospholipids, 3–10% neutral lipids (mainly cholesterol), and 5–10% surfactant-associated proteins. The major phospholipid present is dipalmitoylphosphatidylcholine (DPPC, 30–45%). Other major components are unsaturated phosphatidylcholines (PC, 25–35%), phosphatidylglycerol, and phosphatidylinositol plus other minor components such as phosphatidylethanolamine and sphingomyelin (4–7). Surfactant-associated proteins, SP-B and SP-C, are low molecular weight, hydrophobic proteins that accelerate surfactant adsorption and promote the ability to attain low surface tensions. SP-A and SP-D are hydrophilic glycoproteins. SP-A affects surfactant lipid structure and plays a role in its surface activity by binding DPPC and by enhancing effects due to SP-B (4,8–10).

Cholesterol is the major neutral lipid in pulmonary surfactant with a concentration of up to 10% by mass (20 mol %) (11,12). The presence of cholesterol in surfactant has long been known; however, the role of cholesterol in surfactant remains uncertain. The cholesterol/phospholipid ratio in pulmonary surfactant has been shown to increase slightly as a result of exercise (13), to approximately double during lung injury (14), and to increase by 1.5-fold in heterothermic mammals undergoing torpor (15). It has recently been reported that physiological levels of cholesterol enhance the adsorption of surfactant phospholipids to the equilibrium surface tension of ~23 mN/m (16). Other studies have found that cholesterol enhances adsorption of lipid extract surfactant at 25°C but has no significant effect at physiological temperatures (17). These effects of cholesterol on surfactant adsorption are generally attributed to the fluidizing effects of the sterol on phospholipid mixtures containing relatively high levels of DPPC (18,19). However, phospholipid fluidization could impede the ability of such films to attain low surface tensions during compression.

In keeping with this suggestion, early in vitro functional measurements using a Langmuir-Wilhelmy surface balance and the pulsating bubble surfactometer (PBS) revealed that

Submitted October 19, 2006, and accepted for publication April 11, 2007.

Address reprint requests to Nils O. Petersen, National Institute for Nanotechnology. Tel.: 780-641-1610; Fax: 780-492-8632; E-mail: nils.petersen@nrc-cnrc.gc.ca.

Editor: Thomas Schmidt.

0006-3495/07/08/1391/11 $2.00

doi: 10.1529/biophysj.106.099762

physiological amounts of cholesterol inhibit the ability of surfactant to attain low surface tensions (19–26). Accordingly, cholesterol is removed from many clinically used surfactant extracts. For example, it is extracted from BLES, the clinical surfactant used for these studies. However, it is clear that cholesterol is endogenously present in surfactant, and surface tensions near zero have been measured in the healthy lung (27), indicating that cholesterol does not necessarily interfere with lung function in vivo. The early findings may be related to technical difficulties. Thus, more recent in vitro studies using captive bubble tensiometry (CBT) show that physiological amounts of cholesterol do not affect the surface activity of an artificial surfactant with chemical composition close to natural surfactant (28) or a clinically used surfactant extract (29).

In this study, we seek to relate the effect of cholesterol in vivo with that of cholesterol in vitro and to understand how cholesterol exerts its effects. We studied the physiological effect of cholesterol by monitoring blood oxygenation levels of surfactant-deficient rats treated or not treated with a clinically used exogenous surfactant (bovine lipid extract surfactant, BLES) containing zero or physiological amounts of cholesterol. We use the term ''physiological'' in reference to most homeothermic mammals. We also examined the effect of cholesterol on the surface activity of BLES using CBT. Various amounts of cholesterol (physiological and higher) were added to BLES, and changes in surface tension were observed upon adsorption and during slow compression/expansion (quasistatic) cycles and fast (dynamic) cycles as in normal breathing.

The effect of cholesterol on the topography and lateral organization of BLES Langmuir-Blodgett (LB) films was investigated using atomic force microscopy (AFM). The location of cholesterol in BLES LB films containing various amounts of deuterated cholesterol was determined by time-of-flight-secondary ion mass spectrometry (ToF-SIMS) imaging. Our results show that addition of physiological amounts of cholesterol (20 mol %) does not inhibit the surface activity of BLES at 37°C, whereas higher amounts (50 mol %) greatly decrease its ability to attain low surface tension. Based on our in vivo results, the presence of a physiological amount of cholesterol has no initial effect on blood oxygenation levels. Finally, we show that both physiological and supraphysiological levels of cholesterol induce structural changes in BLES LB films.

MATERIALS AND METHODS

Materials

BLES was a generous gift from BLES Pharmaceuticals (London, Ontario, Canada) and was extracted before use using a modified Bligh and Dyer technique explained elsewhere (30). Extracted BLES was stored in chloroform at −20°C until use. Cholesterol was obtained from Sigma (St. Louis, MO), and cholesterol-25,26,26,26-27,27,27-d7 was purchased from CDN Isotopes (Pointe Claire, Quebec, Canada). Both were received as powders and were dissolved in chloroform at a concentration of 1 mg/mL and stored at −20°C. All solvents used were high-performance liquid chromatography grade and were used without further purification.

Animal experimentation

Male Sprague-Dawley rats (300–500 g) were used for these experiments (Charles River, Saint-Constant, Quebec, Canada). All procedures were approved by the animal use subcommittee of the University of Western Ontario. The physiological response of surfactant-deficient animals to administration of surfactant was determined as previously described (31). Briefly, rats were anaesthetized, connected to a mechanical ventilator, and made surfactant deficient by repetitive saline lavage. Subsequently, animals were randomized into one of three groups: 1), animals receiving 20 mg phospholipid/kg BLES, 2), animals receiving 20 mg phospholipids/kg BLES containing 20 mol % cholesterol, or 3), a nontreated air bolus control group. After treatment the animals were reconnected to the ventilator for an additional 120 min, during which time arterial PO_2 values were determined at 15 min intervals as an indication of the physiological properties of the instilled material. All data are presented as mean ± SE.

Captive bubble tensiometry

The surface activity of the samples was examined by measuring adsorption and by estimating surface tension of bubbles compressed and expanded in quasistatic and dynamic modes using a custom designed CBT (32). CBT experiments were performed in triplicate, using 500-μg/mL samples diluted in buffer (0.150 mM NaCl, 2 mM Tris-HCl, 1.5 mM $CaCl_2$). After the CBT chamber was filled with the desired surfactant in buffer and the temperature equilibrated at 37°C ± 1°C, an air bubble 5–8 mm in diameter was introduced. The change in bubble shape was recorded to monitor the adsorption of the surfactant material to the air-saline interface. After equilibrium surface tension, γ_{eq}, was attained, the chamber was sealed, and quasistatic or dynamic compression-expansion cycles of the bubble were performed. Changes in bubble area were recorded during each individual experiment and the bubble shapes analyzed using custom designed software to calculate the surface tension of the film (32,33).

For quasistatic experiments, the pressure in the sample chamber was increased stepwise by turning the plunger 5–10° (~10% of bubble volume per step) and waiting 10 s for equilibration after each step. Four quasistatic cycles were performed with an intercycle delay of 4 min on return to original volume. The minimum surface tension, γ_{min}, was achieved when the bubble decreased in size without any further flattening on increasing the chamber pressure. Dynamic modes were performed in separate experiments by cycling the bubble at 25 cycles/min. The surface area of the bubble was reduced until the film reached γ_{min} (a value known from quasistatic experiments) and then expanded to 100–120% of original area and cycled between these two limits. All data are presented as mean ± SE.

Langmuir-Blodgett transfer

Surfactant films were prepared by spreading chloroform solutions of BLES containing various amounts of deuterated and nondeuterated cholesterol onto 90 mL of doubly distilled water (pH of 7.0 ± 0.5) in a Langmuir trough (μ-trough-SE by Kibron, Helsinki, Finland) at ambient temperature (24°C ± 1°C). The films were allowed to equilibrate for 10 min before compression at 0.02 nm^2 $molecule^{-1}$ min^{-1} until the desired pressure of 30 mN/m was reached. Monolayer films were deposited onto substrates by elevating the previously submerged substrates vertically through the air-water interface at a rate of 2.0 mm/min. Freshly cleaved mica was used as a substrate for AFM studies, and gold-coated mica was used for ToF-SIMS studies. Gold-coated mica was prepared by inserting freshly cleaved 1 × 1 cm^2 pieces of mica into a Hummer VI sputtering system (Technics EM, Springfield, VA) under reduced pressure at 100 mTorr. The Au was sputtered onto the substrate for

10 min at a plate current of 10 mA. Deposited films were imaged within 2 h of deposition.

Cholesterol depletion

Two procedures were used to extract cholesterol from the surfactant film, both utilizing methyl β-cyclodextrin. In the first procedure, BLES + 20 mol % cholesterol was spread onto 90 mL of 1 mM methyl β-cyclodextrin and incubated for 1 h. The film was then compressed to a surface pressure of 30 mN/m and deposited on mica as described above and imaged by AFM. In the second procedure, BLES + 20 mol % cholesterol was spread onto doubly distilled water and compressed to the desired pressure of 30 mN/m. Concentrated methyl β-cyclodextrin was then introduced in the subphase to give a final concentration of 1 mM. After 1 h incubation, the film was deposited onto mica and imaged by AFM. Results obtained from the two procedures were identical.

Atomic force microscopy

Topographical atomic force microscope images were obtained using a Nanoscope III scanning force multimode microscope (Digital Instruments, Santa Barbara, CA). Samples were scanned in contact mode in air within 2 h of deposition. A silicon nitride cantilever was used with a spring constant of 0.3 N/m, and the scanner was of the J type. Image analysis was performed using the Nanoscope III software (version 5.12r3).

ToF-SIMS imaging

ToF-SIMS images were collected using an ION-TOF ToF-SIMS IV (ION-TOF, Muster, Germany) with a pulsed 25 keV $^{69}Ga^{+}$ primary ion beam in ''burst-alignment'' current mode. This mode uses a pulse width of 200 ns, a spot size in the 250 nm range, and unit mass resolution. All images obtained were 256 × 256 pixels. From previous studies (34), it is known that the static limit for these materials is passed at $\sim 8 \times 10^{12}$ ions/cm^2. Generally, an ion dose of $<5 \times 10^{12}$ ions/cm^2 was used for these analyses (equivalent to ~10 scans for a 100 × 100 μm^2 image at 1 pA primary ion current and 3 scans for a 50 × 50 μm^2 image at 1 pA).

Principal component analysis evaluation

Multi-ion SIMS 1.2 was the software used for principal component analysis (PCA) examination of negative and positive ToF-SIMS images of BLES + 30 mol % cholesterol-d7 samples. As many significant peaks as possible were added to the peak list for analysis. The total remaining ion image (sum of ion intensity not selected as a specific peak) was also added to the peak list since it contains a significant amount of topographic and matrix information. Details of data processing are available elsewhere (34). PCA results are summarized in two ways: a table containing the fragments used in the peak list with corresponding loading value and an image with dimensions of the original image showing the score value of each pixel as a function of position.

RESULTS

The effect of cholesterol on arterial blood oxygenation levels was examined in surfactant-deficient rats. Fig. 1 shows the arterial blood oxygenation values of animals randomized to our three experimental groups. Surfactant-deficient animals that did not receive a surfactant treatment had PaO_2 values that remained low over the entire experimental procedure. Both groups of animals that received exogenous surfactant

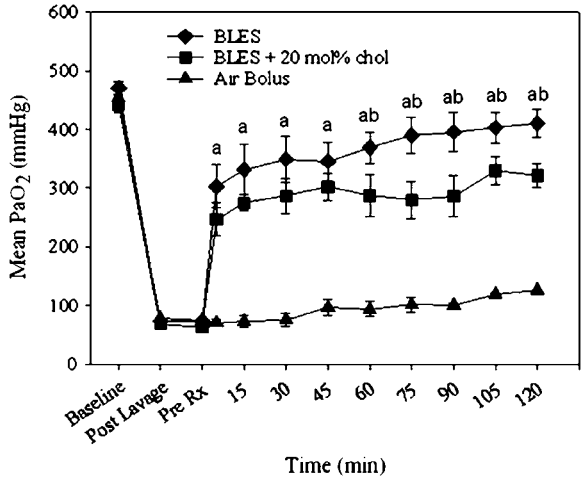

FIGURE 1 Mean arterial blood oxygenation (PaO_2) after air bolus (▲, $n = 5$), 20 mg phospholipids (PL)/kg body weight BLES (♦, $n = 5$) and 20 mgPL/kg BLES + 20 mol % cholesterol (■, $n = 5$). Animals were ventilated with 100% oxygen. $a = p < 0.05$ BLES or BLES + cholesterol versus air bolus, $b = p < 0.05$ BLES versus BLES + cholesterol by two-way ANOVA.

(BLES and BLES + 20 mol % (10% wt/wt) cholesterol), exhibited PaO_2 values that increased significantly immediately after treatment and reached levels significantly higher than the nontreatment group. Comparison of the two treatment groups revealed no significant difference in PaO_2 value immediately after treatment; however during ventilation animals receiving BLES reached higher PaO_2 values than those in the BLES-cholesterol group. The differences were statistically significant at 60 min after ventilation. These results, which indicate a physiological difference between BLES and BLES + cholesterol, prompted us to further investigate the biophysical and structural properties that may be associated with the presence of cholesterol in surfactant.

The biophysical properties, including adsorption and surface tension reduction during both quasistatic and dynamic compression-expansion cycles, were analyzed on a CBT (Figs. 2–4). Adsorption isotherms illustrate how rapidly a substance spreads at the air-water interface to form a film that lowers the surface tension to the equilibrium value. Adsorption isotherms for BLES containing 0, 20, and 50 mol % cholesterol are shown in Fig. 2. BLES containing 0 or 20 mol % cholesterol spread faster than BLES containing 50 mol % cholesterol; however, within 30 min, all films attained equilibrium surface tension, γ_{eq}.

In addition to spreading quickly, a functional surfactant should reach a surface tension close to zero upon subsequent compression. Films at equilibrium were subjected to four quasistatic compression-expansion cycles. Isotherms were prepared and are shown for cycles 1 and 4 in Fig. 3. BLES with and without 20 mol % cholesterol reached low surface tensions (2–5 mN/m) during the initial quasistatic compression. Film compressibility (here defined as the % surface area

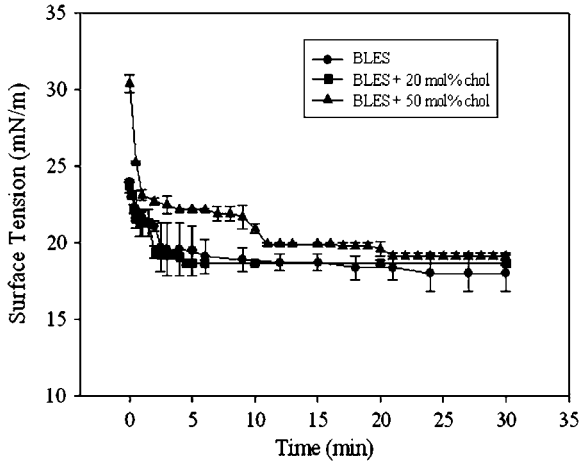

FIGURE 2 Adsorption isotherms of BLES containing increasing amounts of cholesterol. Isotherms were constructed by monitoring adsorption of 500 μg/ml BLES in the absence or presence of cholesterol in the CBT at 37°C.

reduction required to reduce γ from equilibrium to 0 mN/m) was slightly lower with 20 mol % cholesterol. The BLES + 50 mol % cholesterol sample proved incapable of lowering γ below 10 mN/m and film compressibility was high. With all three samples, γ increased dramatically during surface area expansion. BLES and BLES + 20 mol % cholesterol exhibited good respreading once equilibrium γ was attained resulting in γ_{max} levels around 25 mN/m.

The BLES + 50 mol % cholesterol sample showed hampered respreading such that γ_{max} was close to 30 mN/m. Nevertheless, by quasistatic cycle 4, although BLES was able to attain γ-values below 5 mN/m, γ_{min} remained slightly higher than with the 20 mol % sample. In addition, BLES compressibility was slightly greater than with the 20 mol % cholesterol-containing BLES, which required a surface area reduction of ~12% comparable with that of spread DPPC film (4,33). In contrast, the ability of the 50 mol % cholesterol sample to attain low γ did not improve but rather deteriorated, likely as a result of poor PL respreading to equilibrium and instability at low surface tension. The cholesterol-free BLES sample exhibited a small but distinct hysteresis. The BLES containing 20 mol % cholesterol sample demonstrated lowered expandability such that γ during film expansion remained close to the compression values, virtually obliterating hysteresis. This indicates that the resulting film compression-expansion characteristics have become almost perfectly reversible. The high cholesterol sample continued to demonstrate significant hysteresis.

Dynamic compression-expansion cycling permits evaluation of surfactant films under conditions resembling normal breathing (25 cycles/min). All three samples showed some improvement by the 21st cycle. The BLES and BLES + 20 mol % cholesterol samples both attained γ_{min} near 0 and γ_{max} values below 30 mN/m. Although the BLES + 50 mol % cholesterol sample demonstrated the greatest relative improvement, γ_{min} remained high and γ_{max} was >30 mN/m.

The effect of cholesterol on BLES was investigated by determining the effect of this sterol on the structural organization of monolayers of BLES and BLES containing 20 mol % cholesterol deposited on mica. The films were imaged by AFM in contact mode. The pressure-area isotherm for a monolayer of BLES has been previously reported (35). The isotherm shows a continuous, broad coexistence region of

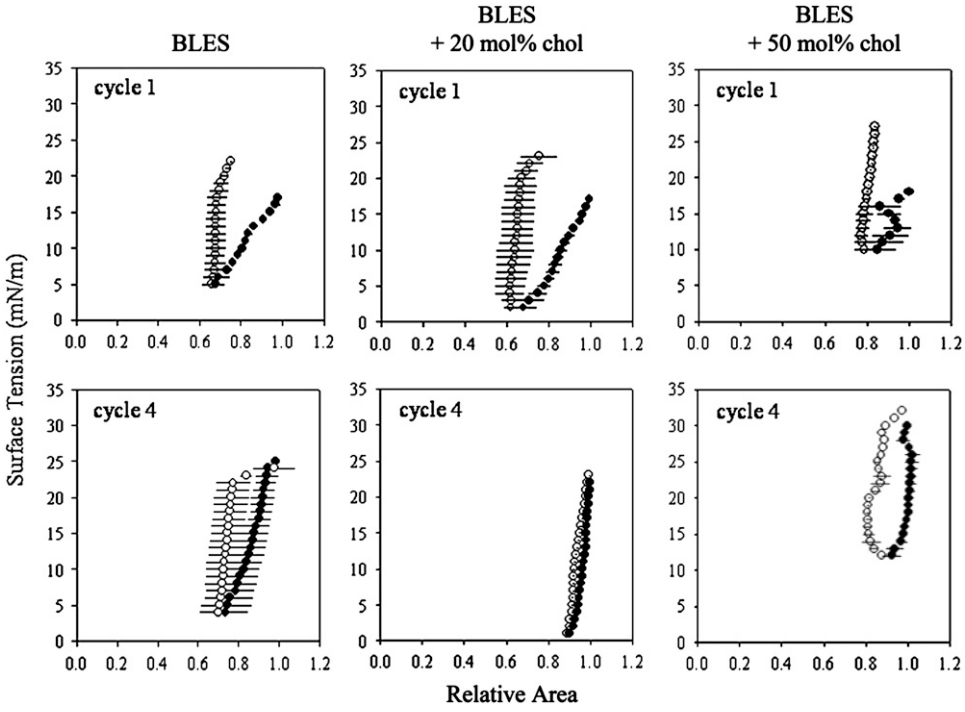

FIGURE 3 Quasistatic compression (●)-expansion (○) isotherms of BLES containing increasing amounts of cholesterol. Isotherms were constructed by averaging three independent experiments for the first and fourth compression-expansion cycles. An intercycle delay of 4 min was used to allow the system to reequilibrate.

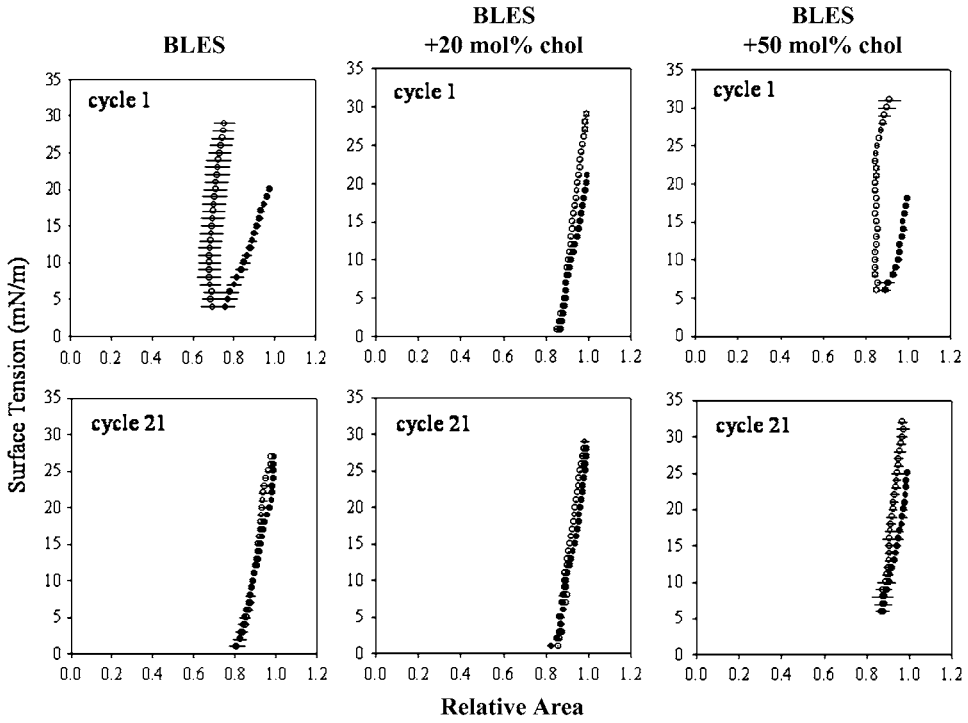

FIGURE 4 Dynamic compression (●)-expansion (○) isotherms of BLES containing increasing amounts of cholesterol. Isotherms were constructed by averaging three independent experiments for the first and 21st compression-expansion cycles. Adsorbed films were cycled at 25 cycles/min.

liquid condensed (LC) and liquid expanded (LE) phases from low pressures to ~42–45 mN/m. All films studied here were deposited onto mica at 30 mN/m, which falls in the normal coexistence region. Fig. 5 *A*, a typical AFM height image obtained for BLES monolayers, shows the presence of circular LC domains in a LE environment. These LC domains form in two sizes: those with an average diameter of ~10 μm microdomains and those with diameters in the range of 100–150 nm nanodomains. Fig. 5 *B* shows that these domains are relatively homogeneous topographically. Height analysis of BLES monolayers (Fig. 5 *C*) shows that the average height of LC micro- and nanodomains are both 0.9 ± 0.01 nm above the surrounding LE phase. The difference in height between LC and LE regions arises from the different composition and molecular tilt of lipids in the two phases.

Fig. 5 *D* is a typical AFM height image for a sample of BLES with 20 mol % cholesterol. In the presence of cholesterol, the number of microdomains increases and the average size decreases (radius ranging 3–6 μm). Nanodomains are still present at similar overall densities and sizes. The presence of cholesterol in BLES also induces the formation of domains within microdomains, as evident in Fig. 5 *E*. Height analysis of these AFM images (Fig. 5 *F*) shows that the height difference between nanodomains and L_d phase is still 0.9 ± 0.01 nm; however, the height difference between new domains within microdomains and the liquid-disordered (L_d) phase is 1.1 ± 0.01 nm (i.e., the new domains rise 0.2 nm above the microdomain). BLES containing cholesterol corresponding to ~10 mol % also yielded AFM images of domains within domains (results not shown).

The role of cholesterol in domain formation was further investigated by removing cholesterol from the surface film. Monolayers of BLES + 20 mol % cholesterol were compressed to a surface pressure of 30 mN/m to allow the formation of domains within domains. A solution of methyl β-cyclodextrin was injected into the subphase since it is known to bind and remove cholesterol from membranes. The monolayer was deposited on mica and imaged by AFM. Fig. 5 *G* shows that both micro- and nanodomains are present, but there are no domains within the microdomains (Fig. 5, *H* and *I*). However, the size of the microdomains increased to 5–10 μm and the number of nanodomains was decreased. Nevertheless, in general, removal of cholesterol by methyl β-cyclodextrin leads to the same phase behavior as BLES without added cholesterol (Fig. 5, *A–C*).

AFM images reveal the structural organization of LB films but not the chemical composition of the different phases. The key question is where is the cholesterol? ToF-SIMS can image the distribution of masses across the sample, thereby providing information about the distribution of chemical species on the surface. However, it is difficult to detect mass fragments uniquely due to cholesterol; so we have resorted to using a specifically deuterium-labeled analog of cholesterol: cholesterol-d7, which contains seven deuterons in the isopropyl group. BLES samples containing 0 and 30 mol % cholesterol-d7 were deposited on gold-coated mica and imaged by ToF-SIMS. The amount of cholesterol was increased from 20 mol % used in AFM studies to 30 mol %

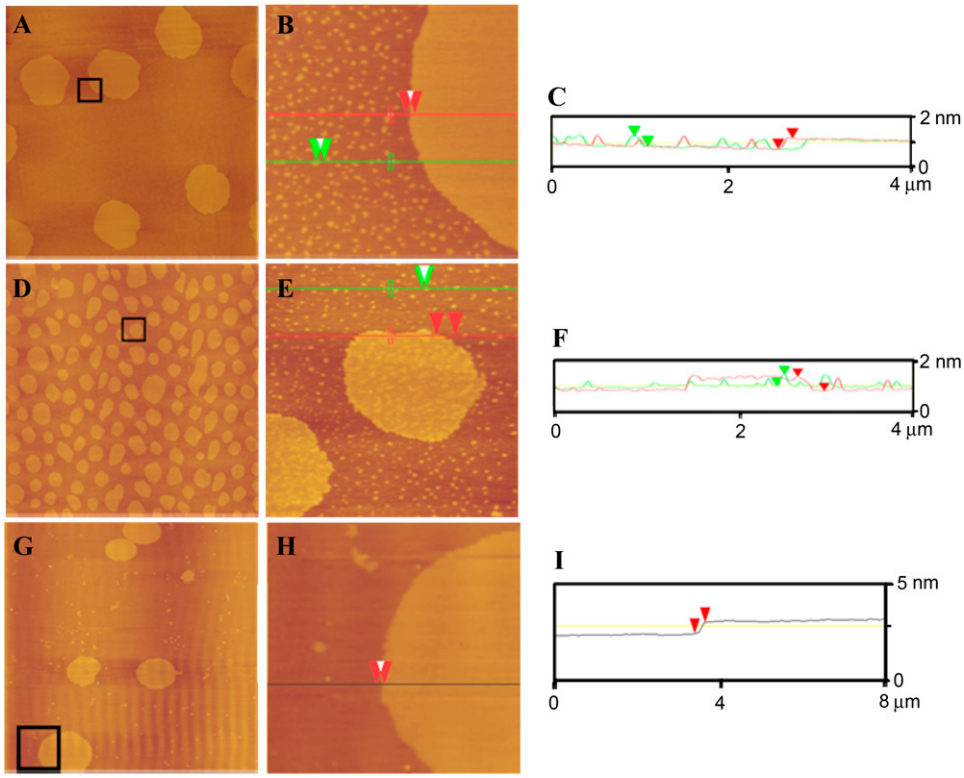

FIGURE 5 AFM height images of BLES (*A* and *B*) and BLES + 20 mol % cholesterol (*D* and *E*). Samples were spread on a liquid-air interface and compressed to a surface pressure of 30 mN/m at 24°C. *G* and *H* are AFM height images of BLES + 20 mol % cholesterol exposed to 1 mM methyl β-cyclodextrin for 1 h at 24°C. Film transfer was performed using the LB method onto mica. The film was scanned in air in contact mode. Images *A*, *D*, and *G* are 60 × 60 μm^2, *B* and *E* are 4 × 4 μm^2, and *H* is 8 × 8 μm^2, and were collected from the boxed areas shown. *C*, *F*, and *I* are height analysis profiles for *B*, *E*, and *H*, respectively, along the lines shown.

in ToF-SIMS studies as an attempt to increase the signal and therefore obtain better images showing the location of cholesterol.

LB films of BLES containing 30 mol % cholesterol-d7 were imaged by AFM and showed similar topographical features as LB films of BLES + 20 mol % cholesterol (results not shown). Imaging in the negative mode (anionic mass fragments), palmitate is detected as the fragment with mass/charge ratio (m/z) 255. The microdomains are seen to contain a large proportion of palmitate (Fig. 6, *A* and *B*), as would be expected if they contain principally DPPC. The diameter of these palmitate-rich domains is similar to that obtained from AFM images of the microdomains. The palmitate signal appears stronger for the BLES sample compared to the BLES + 30 mol % cholesterol-d7 (Fig. 6, *A* and *B*) due to changes in the physical environment of the lipids that contain palmitate. The ToF-SIMS does not have the resolution to detect the nanodomains as individual units.

Reference mass spectra were obtained for pure cholesterol-d7 and BLES in both the positive and negative detection mode to determine specific mass peaks that could be used to identify cholesterol. In the negative ion mode, the only specific fragment with high enough intensity to provide an image with information about the location of cholesterol was at mass/charge ratio (m/z) 2 due to deuterium. Fig. 6 *C* shows the absence of signal when imaging at mass 2 in the negative ion mode of a BLES sample, due to the absence of deuterated cholesterol. In contrast, Fig. 6 *D* shows an intense mass 2 signal from the microdomains, indicating that deuterium, and therefore cholesterol, is highly concentrated in these domains. Based on our ToF-SIMS images, we cannot exclude the possibility that cholesterol is present in the L_d phase as well. Fig. 6, *E–H*, was obtained by subjecting Fig. 6, *A–D*, to a smoothing function that enhances the contrast to more clearly show the location of palmitate and deuterium. Comparison of Fig. 6, *F* and *H*, shows that deuterium is highly concentrated in microdomains of all diameters. At this time we cannot determine whether the cholesterol is present in the domains within the microdomains to a greater or lesser extent.

PCA of 50 × 50 μm^2 negative ion mode images of BLES + 30 mol % cholesterol-d7 resulted in the identification of two principal components (PC1 and PC2) where PC2 gives a very clear image of the two phases. An example of an image score is presented in Fig. 7 *A*, with corresponding factor loadings presented in Fig. 7 *B*. Positive loadings represented graphically in Fig. 7 *B* correspond to mass fragments that are found in the L_d phase. The more positive the loading the stronger the correlation is. Conversely, negative loadings will correspond to mass fragments found in the microdomains. In negative ion mode, strong specific fragments for cholesterol-d7 are found at the following m/z: 2, 77, 232, 233, 391, and 393. The respective loadings for these fragments are negative, indicative of the microdomains. Thus the PCA results also indicate that cholesterol is highly concentrated in the microdomains.

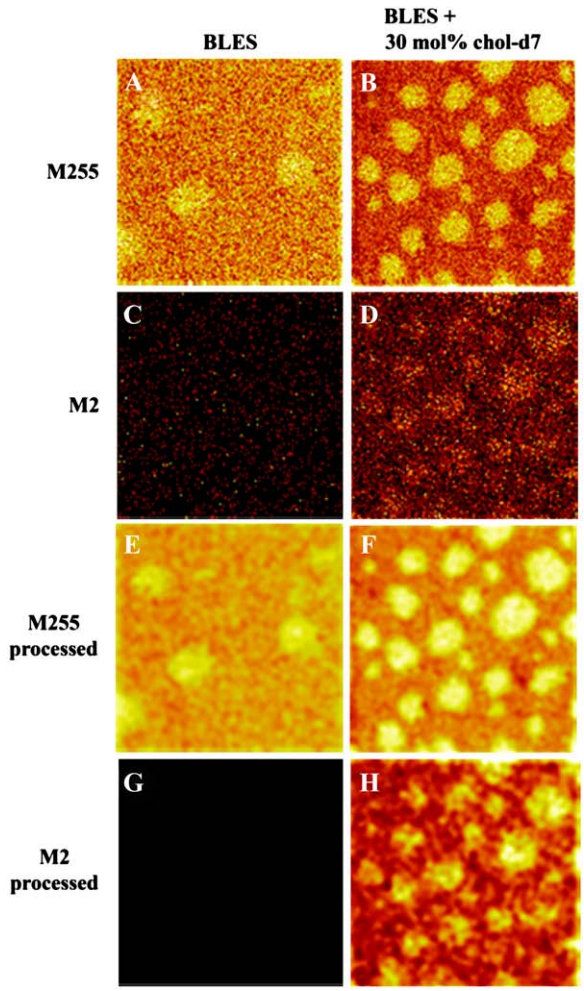

FIGURE 6 ToF-SIMS negative ion images of two BLES LB films containing 0 mol % (*A* and *C*) and 30 mol % (*B* and *D*) cholesterol-d7. M255 corresponds to the palmitate group, M2 to deuterium present in the tail of cholesterol-d7. Images *E–H* were obtained by subjecting *A–D*, respectively, to a smoothing function available as part of the ION-TOF software and show more clearly the location of the palmitate group and deuterium. Images are $50 \times 50\ \mu m^2$, 256×256 pixels with 1 shot/pixel.

AFM height images of monolayers of BLES containing 50 mol % cholesterol deposited at 30 mN/m show the presence of two phases (Fig. 8 *A*). Higher magnification AFM height images were collected (Fig. 8 *B*) which were subjected to height analysis (Fig. 8 *C*) to give a height difference between the two phases of 0.65 ± 0.03 nm. In the presence of high amounts of cholesterol, microdomains ($<10\ \mu m$ in diameter) are still observed as well as large L_o domains that contain holes. ToF-SIMS images were used to determine the location of cholesterol in these samples as well. In the negative ion mode, images of m/z 255 (Fig. 8 *D*) (representing palmitate) show the presence of two phases. Images of m/z 2 (Fig. 8 *E*) (corresponding to deuterium) show that the cholesterol colocalizes with the palmitate—presumably in the more ordered phase. Images shown in Fig. 8, *D* and *E*, were smoothed to enhance the contrast for a better picture of the location of palmitate and deuterium with the results shown in Fig. 8, *F* and *G*.

DISCUSSION

The presence of cholesterol in lung surfactant has long been known. However, its function has remained uncertain. We have attempted to clarify surfactant-cholesterol interactions using in vivo and in vitro biophysical and surface topography approaches. The addition of cholesterol to LC phase phospholipids, such as pure DPPC, results in the formation of a more fluid L_o phase (16,36). Increased fluidity could lead to enhanced adsorption as has been observed with lipid mixtures containing DPPC (18,19,25) and with organic solvent lipid extracts of natural surfactant (16,37). However, although physiological levels of cholesterol-enhanced adsorption of BLES at 24°C, no effect was observed at 37°C (17). In addition, this study showed that the addition of physiological amounts of cholesterol (20 mol %) did not affect BLES adsorption, indicating that BLES fluidity at 37°C was sufficient to support maximal adsorption to the equilibrium surface tension of ~23 mN/m. The basis of the differences in the results obtained by different groups is not understood, but these findings are consistent with the observation that BLES and BLES + 20 mol % cholesterol have similar immediate effects on oxygenation of surfactant-depleted rats (Fig. 1).

The addition of cholesterol to fluid LE PC membranes leads to the formation of L_d phase, which possesses fluidity intermediate between LE and L_o. It is known that cholesterol possesses higher affinity for DPPC than unsaturated PCs (38). However, addition of supraphysiological levels of cholesterol (50 mol %) exceeds the DPPC content of BLES, apparently resulting in the formation of the L_d as well as the L_o phase. Increasing the amount of cholesterol to exceed the maximum DPPC/cholesterol stoichiometry forces the cholesterol to interact with unsaturated phospholipids. This would agree with the work by Bernardino et al. who show that removal of cholesterol from porcine surfactant bilayers leads to a phase transition from fluid ordered/fluid disordered to gel/fluid (16). The decreased adsorption of BLES containing 50 mol % cholesterol (Fig. 2) is consistent with the poor in vivo and in vitro properties of cholesterol-rich surfactant recovered from rats with acute lung injury (14).

Although the increased fluidity arising from cholesterol addition could, at least theoretically, lead to enhancement of surfactant adsorption, it should result in hampered film stability. In keeping with this prediction, the presence of cholesterol greatly diminished the ability of organic solvent lipid extract surfactants to attain low surface tensions near 0 mN/m when assayed with the Langmuir-Wilhelmy surface balance or PBS. For this reason, cholesterol is removed from some natural surfactant-based clinical lipid extract surfactants such as BLES, Curosurf, and Survanta. However, more recent studies using the technically superior CBT have reported that physiological amounts of cholesterol do not alter

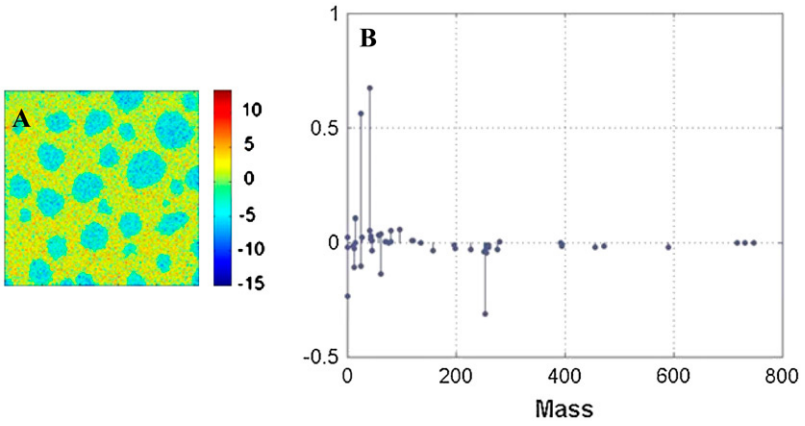

FIGURE 7 (*A*) Image scores for PC2 obtained from PCA of ToF-SIMS negative ion mode images of a BLES + 30 mol % cholesterol-d7 LB film. Image is 50 × 50 μm^2. (*B*) Corresponding loadings for PC2 where negative loadings correspond to the liquid-ordered domains shown in blue, and positive loadings correspond to the liquid-disordered phase shown in yellow.

the biophysical function of surfactant when using materials derived from native surfactant or artificial surfactants of close to natural composition (16,29).

In agreement, our studies found that 20 mol % cholesterol did not affect the initial adsorption kinetics (Fig. 2) and led to slightly lower surface tensions during compression with quasistatic and dynamic in vitro CBT experiments (Figs. 3 and 4). In contrast, high concentrations of cholesterol (50 mol %) clearly had detrimental effects on spreading kinetics as well as the ability to attain low γ-values (Figs. 3 and 4). The observations are consistent with recent studies by Gunasekara et al. (29), who observed that whereas 20 mol % cholesterol did not affect BLES adsorption or the ability to attain low tensions, elevating cholesterol to 40 mol % abolished normal surfactant function. Interestingly, they also found that addition of DPPC to BLES containing high cholesterol so that the stoichiometry of the DPPC/cholesterol complex was restored, recovered the ability of the film to reach low surface tension. Since the level of cholesterol is higher in acutely injured lungs, it is possible that elevated levels of cholesterol could contribute to surfactant failure in acutely injured lungs (14). In these latter studies, cholesterol was present in the functional large aggregate surfactant fraction, indicating that cholesterol was an inherent part of pulmonary surfactant. The cholesterol content of large aggregate fraction increased with lung injury, suggesting the increase in cholesterol was not attributable to the influx of lipoproteins. Nevertheless, this possibility remains an important area for further research.

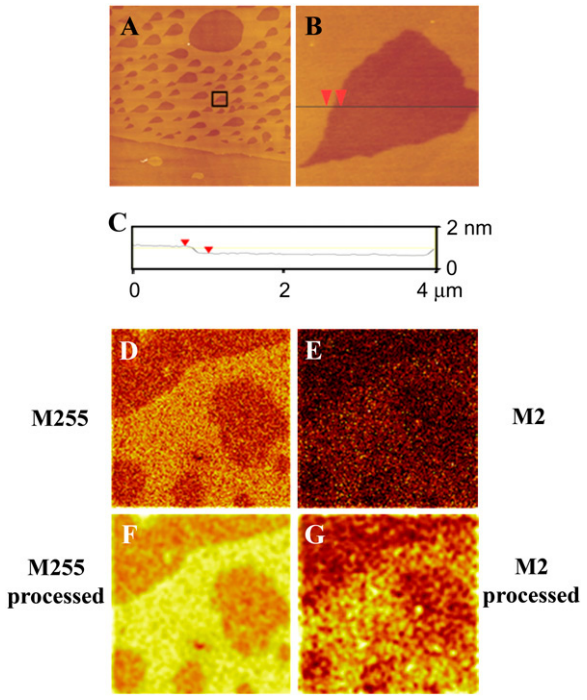

FIGURE 8 (*A* and *B*) AFM height images of BLES + 50 mol % cholesterol. Samples were spread on a liquid-air interface and compressed to a surface pressure of 30 mN/m at 24°C. Film transfer was performed using the LB method onto mica. The film was scanned in air in contact mode. Image *A* is 60 × 60 μm^2 and *B* is 4 × 4 μm^2 and was collected from the boxed area shown in *A*. *C* is a height analysis profile for *B* along the line shown. (*D* and *E*) ToF-SIMS negative ion images of BLES + 50 mol % cholesterol-d7. M255 corresponds to the palmitate group, M2 to deuterium present in the tail of cholesterol-d7. Images *F* and *G* were obtained by subjecting *A* and *B*, respectively, to a smoothing function available as part of the ION-TOF software and show more clearly the location of the palmitate group and deuterium. Images *D*–*G* are 50 × 50 μm^2, 256 × 256 pixels with 1 shot/pixel.

In the past, surfactant function has been explained by the generation of a surfactant monolayer which becomes highly enriched in the gel phase lipid DPPC during repeated compression-expansion cycling. More recent studies provide evidence indicating that surfactant may function as a multilayer, rather than a monolayer (5,29,33,39–41). Moreover, under certain conditions the pure fluid phospholipid, 1-palmitoyl, 2-oleoyl phosphatidylcholine (POPC), can attain surface tensions near zero at 37°C (36,42–45). Thus solid LC phase lipids such as DPPC are not absolutely necessary for a monolayer to attain near zero surface tension at physiological temperatures in vitro. On the basis of these results we propose that the ability of surfactant to withstand sufficient surface pressure to attain near zero surface tension depends on dynamic surfactant film organization rather than on dynamic alterations in surface film composition, such as DPPC

enrichment. We have employed AFM and ToF-SIMS to examine organization in the presence and absence of cholesterol.

Two interesting observations were made during AFM studies of surfactant films in the presence of physiological amounts of cholesterol. First, there was an increase in the number of microdomains and a decrease in their size (Fig. 5 *D*). Second, there was the formation of new domains within the microdomains (Fig. 5 *E*) with a height difference of ~0.2 nm. The effects observed are due to cholesterol since its removal with methyl β-cyclodextrin removes the domains within the microdomains and also leads to the formation of fewer, larger microdomains (Fig. 5, *G* and *H*). The change in domain size after addition of cholesterol could be a kinetic or thermodynamic effect. The addition of cholesterol could lead to an increase in the number of nucleation sites, which could lead to the formation of more domains. Addition of cholesterol could also lead to a decrease in line tension, which could also explain the formation of more, smaller domains. We consider the latter explanation to be more likely.

The observed height difference in our AFM data would most likely be due to the interaction between cholesterol and DPPC, which leads to an increased ordering of the hydrocarbon chains of this phospholipid. The formation of domains within the microdomains is not a result of protein aggregation since the same effect was observed when 20 mol % cholesterol was added to a mixture of 50:30:20 DPPC/POPC/POPG (E. Keating, R. Veldhuizen, F. Possmayer, and N. O. Petersen, unpublished data). Based on our ToF-SIMS results, it appears that the cholesterol is concentrated in the microdomains. At this stage, however, it is impossible to determine whether cholesterol is preferentially in the domains within the microdomains. It is possible that some cholesterol is located in the nanodomains even though we did not observe an increase in the height of these domains in the presence of cholesterol. This could be due to the small amount of cholesterol present here, which may not induce a detectable height difference.

Our finding of cholesterol in L_o domains agrees with the composition of lipid rafts found in mammalian plasma membranes. Rafts are liquid domains enriched in cholesterol, saturated long-chain phospholipids, and certain proteins and play important roles in various cellular functions such as signaling and endocytosis (46–48). Our results also agree with a previous AFM study where LB films of DPPC + cholesterol were shown to be thicker than DPPC films alone (49). It is accepted that saturated phospholipids like DPPC are present in the LC domains, whereas the main constituents of the more fluid LE phase are unsaturated phospholipids like POPC and POPG. Additions of cholesterol to phospholipids result in the formation of intermediate L_o phases within DPPC and with high cholesterol L_d phases in the case of unsaturated fluid phospholipids. Interestingly, as we increased the concentration of cholesterol to 50 mol %, the percolation threshold was crossed and the large L_o domains became connected with L_d islands trapped within (Fig. 8 *A*). Despite being continuous, these large L_o domains are not sufficiently stable to allow compression to low surface tension on the CBT (Fig. 4).

Our AFM data provide information about changes in the structural organization of surfactant at the surface upon cholesterol addition; however, they provide no information about the location of cholesterol in the films. Recently, ToF-SIMS imaging techniques have been used to obtain chemical maps of deposited monolayer films with submicron resolution. Here, we added deuterated-cholesterol to BLES and used the m/z 2 in negative ion mode to identify the location of cholesterol. Since there is no other source of mass units of two in negative ion mode, we conclude that cholesterol is highly enriched in the microdomains (Fig. 6, *D* and *H*). The signal is too weak to establish whether cholesterol is present specifically in the domains within microdomains. Our PCA results confirm that cholesterol is enriched in the microdomains where it remains even at elevated levels of 50 mol % cholesterol (Fig. 8, *E* and *G*).

CONCLUSION

Our studies show that, although physiological levels of cholesterol do not interfere and may slightly improve the in vitro biophysical properties of BLES, this preparation lacks the ability to maintain good gas exchange in surfactant-deficient rats. We speculate that the change in PaO_2 over time is due to the way BLES + cholesterol is handled in the airspace rather than its biophysical properties. This area needs further investigation. It has been shown that the level of cholesterol increases after acute lung injury. We show that surfactant containing supraphysiological amounts of cholesterol loses its ability to reach low surface tension. Our AFM results provide information about the lateral organization of BLES films containing no, physiological, and supraphysiological amounts of cholesterol. These results indicate that addition of cholesterol leads to the formation of a highly ordered L_o phase which slightly improves the activity of BLES. However, addition of cholesterol to exceed the amount of saturated PL leads to the formation of L_d which has a detrimental effect on the activity of surfactant.

The authors thank BLES Biochemicals, London, Ontario for generously providing BLES.

This work has been supported by Canadian Institute of Health Research Operating Grant MOP64406.

REFERENCES

1. Gunther, A., C. Ruppert, R. Schmidt, P. Markart, F. Grimminger, D. Walmrath, and W. Seeger. 2001. Surfactant alteration and replacement in acute respiratory distress syndrome. *Respir. Res.* 2:353–364.
2. Lewis, J. F., and R. Veldhuizen. 2003. The role of exogenous surfactant in the treatment of acute lung injury. *Annu. Rev. Physiol.* 65: 613–642.

3. Robertson, B., and H. L. Halliday. 1998. Principles of surfactant replacement. *Biochim. Biophys. Acta.* 1408:346–361.
4. Possmayer, F. 1997. Physicochemical aspects of pulmonary surfactant. *In* Fetal and Neonatal Physiology. R. A. Polin and W. W. Fox, editors. Saunders, Philadelphia. 1259–1275.
5. Postle, A. D., E. L. Heeley, and D. C. Wilton. 2001. A comparison of the molecular species compositions of mammalian lung surfactant phospholipids. *Comp. Biochem. Physiol. A Mol. Integr. Physiol.* 129: 65–73.
6. Schiller, J., S. Hammerschmidt, H. Wirtz, J. Arnhold, and K. Arnold. 2001. Lipid analysis of bronchoalveolar lavage fluid (BAL) by MALDI-TOF mass spectrometry and ^{31}P NMR spectroscopy. *Chem. Phys. Lipids.* 112:67–79.
7. Veldhuizen, R., K. Nag, S. Orgeig, and F. Possmayer. 1998. The role of lipids in pulmonary surfactant. *Biochim. Biophys. Acta.* 1408:90–108.
8. Cockshutt, A. M., J. Weitz, and F. Possmayer. 1990. Pulmonary surfactant-associated protein A enhances the surface activity of lipid extract surfactant and reverses inhibition by blood proteins in vitro. *Biochemistry.* 29:8424–8429.
9. Rodriguez-Capote, K., K. Nag, S. Schurch, and F. Possmayer. 2001. Surfactant protein interactions with neutral and acidic phospholipid films. *Am. J. Physiol. Lung Cell. Mol. Physiol.* 281:L231–L242.
10. Venkitaraman, A. R., S. B. Hall, J. A. Whitsett, and R. H. Notter. 1990. Enhancement of biophysical activity of lung surfactant extracts and phospholipid-apoprotein mixtures by surfactant protein A. *Chem. Phys. Lipids.* 56:185–194.
11. Casals, C., J. Arias-Diaz, F. Valino, A. Saenz, C. Garcia, J. L. Balibrea, and E. Vara. 2003. Surfactant strengthens the inhibitory effect of C-reactive protein on human lung macrophage cytokine release. *Am. J. Physiol. Lung Cell. Mol. Physiol.* 284:L466–L472.
12. Orgeig, S., and C. B. Daniels. 2001. The roles of cholesterol in pulmonary surfactant: insights from comparative and evolutionary studies. *Comp. Biochem. Physiol. A Mol. Integr. Physiol.* 129:75–89.
13. Doyle, I. R., M. E. Jones, H. A. Barr, S. Orgeig, A. J. Crockett, C. F. McDonald, and T. E. Nicholas. 1994. Composition of human pulmonary surfactant varies with exercise and level of fitness. *Am. J. Respir. Crit. Care Med.* 149:1619–1627.
14. Panda, A. K., K. Nag, R. R. Harbottle, K. Rodriguez-Capote, R. A. W. Veldhuizen, N. O. Petersen, and F. Possmayer. 2004. Effect of acute lung injury on structure and function of pulmonary surfactant films. *Am. J. Respir. Cell Mol. Biol.* 30:641–650.
15. Codd, J. R., N. C. Slocombe, C. B. Daniels, P. G. Wood, and S. Orgeig. 2000. Periodic fluctuations in the pulmonary surfactant system in Gould's wattled bat (*Chalinolobus gouldii*). *Physiol. Biochem. Zool.* 73:605–612.
16. Bernardino de la Serna, J. Perez-Gil, A. C. Simonsen, and L. A. Bagatolli. 2004. Cholesterol rules: direct observation of the coexistence of two fluid phases in native pulmonary surfactant membranes at physiological temperatures. *J. Biol. Chem.* 279:40715–40722.
17. Yu, S. H., and F. Possmayer. 1993. Adsorption, compression and stability of surface films from natural, lipid extract and reconstituted pulmonary surfactants. *Biochim. Biophys. Acta.* 1167:264–271.
18. Daniels, C. B., H. A. Barr, J. H. Power, and T. E. Nicholas. 1990. Body temperature alters the lipid composition of pulmonary surfactant in the lizard Ctenophorus nuchalis. *Exp. Lung Res.* 16:435–449.
19. Notter, R. H., S. A. Tabak, and R. D. Mavis. 1980. Surface properties of binary mixtures of some pulmonary surfactant components. *J. Lipid Res.* 21:10–22.
20. Fleming, B. D., and K. M. Keough. 1988. Surface respreading after collapse of monolayers containing major lipids of pulmonary surfactant. *Chem. Phys. Lipids.* 49:81–86.
21. Hildebran, J. N., J. Goerke, and J. A. Clements. 1979. Pulmonary surface film stability and composition. *J. Appl. Physiol.* 47:604–611.
22. Suzuki, Y. 1982. Effect of protein, cholesterol, and phosphatidylglycerol on the surface activity of the lipid-protein complex reconstituted from pig pulmonary surfactant. *J. Lipid Res.* 23:62–69.
23. Taneva, S., and K. M. Keough. 1997. Cholesterol modifies the properties of surface films of dipalmitoylphosphatidylcholine plus pulmonary surfactant-associated protein B or C spread or adsorbed at the air-water interface. *Biochemistry.* 36:912–922.
24. Yu, S., P. G. Harding, N. Smith, and F. Possmayer. 1983. Bovine pulmonary surfactant: chemical composition and physical properties. *Lipids.* 18:522–529.
25. Yu, S. H., and F. Possmayer. 1994. Effect of pulmonary surfactant protein A (SP-A) and calcium on the adsorption of cholesterol and film stability. *Biochim. Biophys. Acta.* 1211:350–358.
26. Yu, S. H., and F. Possmayer. 1998. Interaction of pulmonary surfactant protein A with dipalmitoylphosphatidylcholine and cholesterol at the air/water interface. *J. Lipid Res.* 39:555–568.
27. Schurch, S. 1982. Surface tension at low lung volumes: dependence on time and alveolar size. *Respir. Physiol.* 48:339–355.
28. Diemel, R. V., M. M. Snel, L. M. Van Golde, G. Putz, H. P. Haagsman, and J. J. Batenburg. 2002. Effects of cholesterol on surface activity and surface topography of spread surfactant films. *Biochemistry.* 41:15007–15016.
29. Gunasekara, L., S. Schurch, W. M. Schoel, K. Nag, Z. Leonenko, M. Haufs, and M. Amrein. 2005. Pulmonary surfactant function is abolished by an elevated proportion of cholesterol. *Biochim. Biophys. Acta.* 1737:27–35.
30. Nag, K., J. Perez-Gil, M. L. Ruano, L. A. Worthman, J. Stewart, C. Casals, and K. M. Keough. 1998. Phase transitions in films of lung surfactant at the air-water interface. *Biophys. J.* 74:2983–2995.
31. Bailey, T. C., E. L. Martin, L. Zhao, and R. A. Veldhuizen. 2003. High oxygen concentrations predispose mouse lungs to the deleterious effects of high stretch ventilation. *J. Appl. Physiol.* 94:975–982.
32. Schurch, S., H. Bachofen, J. Goerke, and F. Possmayer. 1989. A captive bubble method reproduces the in situ behavior of lung surfactant monolayers. *J. Appl. Physiol.* 67:2389–2396.
33. Schurch, S., F. H. Green, and H. Bachofen. 1998. Formation and structure of surface films: captive bubble surfactometry. *Biochim. Biophys. Acta.* 1408:180–202.
34. Biesinger, M. C., P. Y. Paepegaey, N. S. McIntyre, R. R. Harbottle, and N. O. Petersen. 2002. Principal component analysis of TOF-SIMS images of organic monolayers. *Anal. Chem.* 74:5711–5716.
35. Harbottle, R. R., K. Nag, N. S. McIntyre, F. Possmayer, and N. O. Petersen. 2003. Molecular organization revealed by time-of-flight secondary mass spectrometry of a clinically used extracted pulmonary surfactant. *Langmuir.* 19:3698–3704.
36. Piknova, B., V. Schram, and S. B. Hall. 2002. Pulmonary surfactant: phase behavior and function. *Curr. Opin. Struct. Biol.* 12: 487–494.
37. Notter, R. H., D. P. Penney, J. N. Finkelstein, and D. L. Shapiro. 1986. Adsorption of natural lung surfactant and phospholipid extracts related to tubular myelin formation. *Pediatr. Res.* 20:97–101.
38. Lund-Katz, S., H. M. Laboda, L. R. McLean, and M. C. Phillips. 1988. Influence of molecular packing and phospholipid type on rates of cholesterol exchange. *Biochemistry.* 27:3416–3423.
39. Possmayer, F., K. Nag, K. Rodriguez, R. Qanbar, and S. Schurch. 2001. Surface activity in vitro: role of surfactant proteins. *Comp. Biochem. Physiol. A Mol. Integr. Physiol.* 129:209–220.
40. Schurch, S., H. Bachofen, and F. Possmayer. 2001. Surface activity in situ, in vivo, and in the captive bubble surfactometer. *Comp. Biochem. Physiol. A Mol. Integr. Physiol.* 129:195–207.
41. Veldhuizen, E. J., and H. P. Haagsman. 2000. Role of pulmonary surfactant components in surface film formation and dynamics. *Biochim. Biophys. Acta.* 1467:255–270.
42. Smith, E. C., J. M. Crane, T. G. Laderas, and S. B. Hall. 2003. Metastability of a supercompressed fluid monolayer. *Biophys. J.* 85: 3048–3057.
43. Crane, J. M., G. Putz, and S. B. Hall. 1999. Persistence of phase coexistence in disaturated phosphatidylcholine monolayers at high surface pressures. *Biophys. J.* 77:3134–3143.

44. Crane, J. M., and S. B. Hall. 2001. Rapid compression transforms interfacial monolayers of pulmonary surfactant. *Biophys. J.* 80:1863–1872.

45. Laderas, T. G., E. C. Smith, J. Crane, and S. B. Hall. 2002. Persistent metastability of rapidly compressed monolayers at the air-water interface. *Biophys. J.* 82:152A. (Abstr.)

46. Brown, D. A., and E. London. 1998. Structure and origin of ordered lipid domains in biological membranes. *J. Membr. Biol.* 164:103–114.

47. Jacobson, K., and C. Dietrich. 1999. Looking at lipid rafts? *Trends Cell Biol.* 9:87–91.

48. Simons, K., and E. Ikonen. 1997. Functional rafts in cell membranes. *Nature.* 387:569–572.

49. Yuan, C., and L. J. Johnston. 2002. Phase evolution in cholesterol/DPPC monolayers: atomic force microscopy and near field scanning optical microscopy studies. *J. Microsc.* 205:136–146.